Edge- and Divertor Plasma Behavior in High Power High Performance Double-null Plasmas on DIII-D

T.W. Petrie[1], M.E. Fenstermacher[2], T. Osborne[1], S.L. Allen[2], H.Y. Guo[1], J.R. Ferron[1], R.J. Groebner[1], C. T. Holcomb[2], A.W. Hyatt[1], C.J. Lasnier[2], A.W. Leonard[1], T.C. Luce[1], A.G. McLean[2], M. Makowski[2], D. Pace[1], W.M. Solomon[1], F. Turco[3], M. Van Zeeland[1], and J.G. Watkins[4]

[1]*General Atomics, P.O. Box 85608, San Diego, CA 92186-5608, USA.*
[2]*Lawrence Livermore National Laboratory, Livermore, CA 94550, USA.*
[3]*Columbia University, New York, NY 10027, USA.*
[4]*Sandia National Laboratories, P.O. Box 969, Livermore, CA 94551, USA*

e-mail contact of main author: petrie@fusion.gat.com

Abstract. We identify significant opportunities and challenges to reducing divertor heat flux in high power, high performance near-double null divertor (DND) plasmas on DIII-D, while still maintaining a sufficiently low enough density that allows for the application of ECH heating. For these DNDs, the scaling of the peak heat flux at the outer target ($q_{\perp}^{P}$) $\propto$ [P_{SOL} x I_P] $^{0.92}$ for P_{SOL} = 8 -19 MW and I_P = 1.0–1.4 MA, and is consistent with standard ITPA scaling for single-null H-mode plasmas. Two divertor heat flux reduction methods were studied. First, the *puff-and-pump radiating divertor* at lower power input (≤11 MW) was effective in reducing divertor heat flux with modest degradation in core confinement. For these plasmas, argon is more effective than nitrogen as the seed impurity, because the former leads to less fuel dilution for similar divertor heat flux reduction. However, puff-and-pump was less effective in reducing $q_{\perp}^{P}$ at high power (≥ 14 MW) and H98 (≥ 1.5) due to an *improvement* in confinement time when deuterium gas puff was applied. Our analysis to-date indicates that this improved energy confinement arises from a complex interplay between pedestal density and temperature profiles and particle transport, resulting in improved edge stability. Second, $q_{\perp}^{P}$ for these high performance DNDs could be lowered by ≈35% when an open divertor was closed on the common flux side of the outer divertor target ("semi-slot"). However, plasma interaction with graphite tiles near the slot opening was a significant source for impurity contamination of the main plasma.

1. Introduction

A future DEMO or commercially-successful tokamak will exploit the highly shaped double-null divertor (DND) concept in order to access the high energy confinement and plasma beta required for successful operation. It would also have to safely exhaust very high levels of power outflow to their divertors. Several approaches have been put forward as potential solutions. Included among them, for example, are the "puff-and-pump" radiating divertor [1-4], reconfiguring the divertor flux surfaces (e.g., poloidal flux expansion at the divertor target [5] or elongating the outer divertor leg allowing for additional heat flow dissipation between the X-point and the divertor target [6]), and applying sophisticated but technically more challenging avenues that use exotic shaping of the divertor legs, such as in the Snowflake [7,8], X-Divertor, and Super-X divertor [9]. Alternatively, the divertor structure itself can be contoured to physically enclose the divertor legs (i.e., "slot divertor"), thereby dissipating power inflow by increasing both radiated power and momentum losses along the enclosed field lines due to enhanced particle trapping.

While these approaches may reduce divertor heat flux to tolerable levels in contemporary highly powered, high performance DND tokamaks, such as DIII-D, the cost in plasma performance in doing so is uncertain. In this paper, we examine this question by applying two of the above techniques (i.e., radiating divertor and partial divertor closure) to high performance DND DIII-D plasmas. With respect to the puff-and-pump radiating divertor, we find that injecting deuterium gas into these highly powered DND plasmas appears to open up a new avenue for achieving elevated plasma performance but may also compromise its

effectiveness in reducing divertor power loading.

In section 2, we describe the experimental arrangement and representative plasma parameters used in this study. In section 3.1 we evaluate the dependence of the divertor peak heat flux for the DND on plasma current and power input. In section 3.2 we compare the differences in puff-and-pump radiating divertor operation with nitrogen or argon as seed impurities. In section 3.3 we examine the improved energy confinement that occurs when deuterium gas D_2 is injected into very highly powered DND plasmas. In section 3.4 we show that partial baffling ("semi-slot") of the lower divertor leg can produce significant heat flux reduction with little loss in plasma performance. We also demonstrate that plasma interaction at the entrance to the slot can lead to significant contamination of the core plasma. In section 4, we offer our conclusions and point out directions for future research.

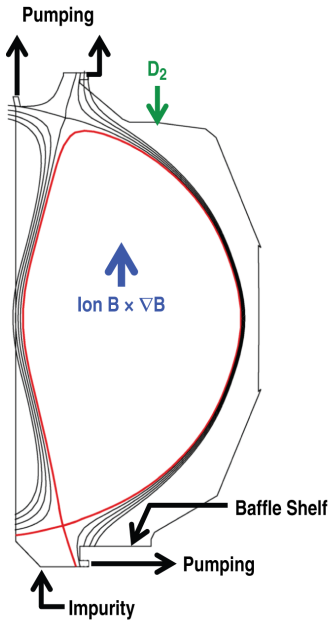

*FIG. 1. The unbalanced double-null plasma configuration used in this study is biased downward (dR_{SEP} = -6 mm) and the **B** x∇B drift direction toward the upper (secondary) divertor. Particles are exhausted from cryopumps at three poloidal locations. Deuterium (D_2) and impurities (IMP) are injected from single poloidal locations, as shown.*

2. Experimental Arrangement

We exploit the plasma shaping capabilities of DIII-D to produce the high triangularity, magnetically unbalanced double-null divertor (DND) shapes commonly associated with elevated energy confinement and β_N, as shown in Fig. 1. These plasmas are characterized by (1) a slight magnetic bias toward the lower divertor, e.g., dRsep = - 5 to -7 mm, (2) the ion **B** x ∇B drift direction toward the upper (secondary) divertor, (3) particle exhaust of deuterium and impurities by cryo-pumping from three poloidal locations, and (4) D_2 gas introduced from the top into the main chamber on the low-field side and seed impurities from a single location in the private flux region of the lower (primary) divertor.

The ELMing hybrid plasmas considered in this study are "high performance", characterized by high energy confinement (e.g., H98 ≥ 1.5) and β_N (≥ 2.5). Representative plasma parameters in this study were: I_P = 1.0–1.4 MA, q_{95} = 4.7–6.5, and total power input (P_{IN}) = 9 - 20 MW, where neutral beams (NB) and applied electron cyclotron heating (ECH) provide plasma heating of up to 16.5 MW and 3.5 MW, respectively. To avoid cutoff/reflection during ECH injection, line-averaged density was constrained to ≤ 5.5 x 10^{19} m^{-3} (or ≤ 0.6 that of the Greenwald density).

Since the interior of the DIII-D vessel is protected by graphite tiles, carbon is the main intrinsic impurity. Heat flux profiles in the *lower* divertor are based on infrared (IR) camera measurements with views perpendicular to the divertor floor, as illustrated in the inset to Fig. 2. A second infrared camera provides a wide-angle field-of-view of the plasma cross-section and divertor and can measure surface temperature in the lower and upper outer divertors and on the outer midplane simultaneously. A tangential view of the lower divertor is also provided by a camera capable of imaging at selected wavelengths. Electron density and temperature at the divertor targets are determined from fixed Langmuir probe measurements, while upstream and pedestal densities and temperatures are based on Thomson scattering. Unless otherwise stated, all measurements quoted above are *between* ELMing events.

3. Results

3.1 Peak heat flux scaling

Figure 2 shows the peak heat flux ($q_{\perp OD}^{P}$) at the outer divertor target in the dominant (lower) divertor as a function of the power flow into the scrape-off layer (P_{SOL}), defined as the power input into the plasma less the radiated power from the core plasma. The outer divertor strike point is well away from the lower baffle structure (≈10 cm), so that the divertor geometry is relatively "open". Three plasma currents are considered. We find that:

$$q_{\perp OD}^{P} \propto [P_{SOL} \times I_P]^{0.92} \qquad (1)$$

These results are largely in-line with predictions from standard ITPA scaling [10]. The latter scaling largely pertains to more conventional single null divertor (SND) configurations, where the **B** x ∇B ion drift is predominantly directed toward the main (only) divertor, e.g., $q_{\perp OD}^{P} \propto [P_{SOL}]^{0.9} \times [I_P]^{1.1}$

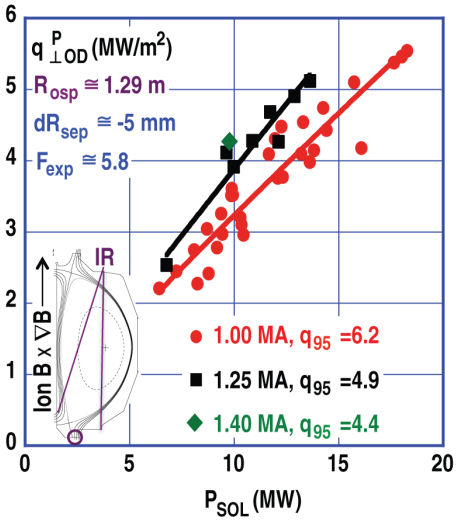

FIG. 2. The peak heat flux at the outer target of the lower divertor ($q_{\perp OD}^{P}$) is plotted as a function power flow into the scrape-off layer (P_{SOL}) for three plasma currents (I_P). A vertical slice at P_{SOL}=10 MW provides the I_P dependence of $q_{\perp}^{P}$. Data is taken between (type-1) ELMing events. The solid curves are the best fit to the data. The inset shows the infrared (IR) camera field-of-view of the divertor target. The power into the main plasma is supplied by both neutral beam and ECH. F_{exp} is the poloidal flux expansion at the outer strike point.

3.2 High performance plasmas at moderate power input

The puff-and-pump radiating divertor has been shown on DIII-D to be a viable approach for reducing divertor heat flux in high performance DND hybrid and high-q_{min} plasmas [4,5], often with only modest degradation in H98. Central and pedestal electron temperatures representative of these highly powered high performance DND plasmas typically fall in the range of 3-5 keV and 1-2 keV, respectively. Electron temperature and $q_{\perp OD}^{P}$ at the divertor targets can reach as high as 50-60 eV and 5 MW/m^2, respectively. Thus, selection of the impurity "seed" that is appropriate for these kinds of plasmas is an important consideration.

Neon, nitrogen, and argon have previously been used as seeds in high power DIII-D experiments, and each was seen to have its strengths and drawbacks. Here we directly compare an argon-based puff-and-pump with one that is nitrogen-based. Table 1 shows four shot types: (1) *D_2 only shot*, i.e., Γ_{D2} = 40 torr l/s, (2) *D_2 + nitrogen shot*, i.e., same Γ_{D2} and

TABLE 1: EFFECTIVENESS OF PUFF-AND-PUMP OPERATION WITH NITROGEN AND ARGON.

Case	D_2 only (165477)	$D_2 + N_2$ (166094)	D_2 + Argon (166098)	Control shot (160714)
P_{IN} (MW)	10.4	10.6	10.6	10.6
n_e (10^{19} m^{-3})	3.92	3.92	4.08	3.83
β_N	2.35	2.49	2.65	2.90
H98	1.16	1.22	1.31	1.45
$P_{R,INSEP}$ (MW)	0.95	1.15	1.64	0.90
$P_{R,OUTSEP}$ (MW)	2.25	4.27	3.28	2.10
$q_{\perp OD}^{P}$ (MW/m^2)	2.1	1.6	1.6	3.0
n_D/n_e (ρ=0.3-0.8)	0.87	0.57	0.77	0.86

Γ_{N2} = 20 torr l/s, (3) *D_2 + argon*, i.e., same Γ_{D2} and Γ_{Ar} = 2.7 torr l/s, and (4) *Control shot*, i.e., only enough D_2 to maintain density. These four cases have virtually the same geometry and global characteristics: I_P = 1 MA, q95 = 5.9, dRsep = -5.5 – -7.0 mm, and little variation in either P_{IN} or line-averaged density (Table 1). In the control shot, β_N is 2.9, but when 40 torr l/s of deuterium was added, β_N dropped almost 20%. This drop, however, was mitigated by the addition of N_2 or argon mostly from higher ion temperatures, with argon providing the larger "recovery". H98 also improved with impurity injection, even though the power radiated inside the separatrix ($P_{R,INSEP}$) was measurably higher in the impurity-injected cases. Higher H98 when impurities were added to D_2 fueling was largely due to higher ion temperature (and lower ion thermal diffusivity) in the impurity-seeded cases.

While nitrogen did not play a major role in the power balance inside the separatrix compared with argon, nitrogen was by far the stronger radiator outside the separatrix ($P_{R,OUTSEP}$). Yet, the net result is that both argon and nitrogen cases provided the same factor of 2 reduction in $q_{\perp OD}^{P}$, when compared with the control case. What gives argon an edge over nitrogen in these high powered high performance DND plasmas is that, fuel dilution of the core plasma was considerably less in the argon case for the same heat flux reduction. Similar behaviors were observed when argon was compared with the other low-Z impurity neon.

3.3 High performance plasmas at high power input

While the "puff-and-pump" radiating divertor was generally effective in reducing divertor heat flux, we have found, however, that this approach is more problematic when P_{IN} is at very high levels. Figure 3(a) shows H98 for a moderately-heated (i.e., 10.3 MW) DND decreased as line-averaged density was raised by D_2 injection, as expected. At higher P_{IN} (i.e., 14.3 MW), however, Fig. 3(a) indicates that H98 *increased* as density was raised, which was not expected. This behavior may be tied to the how ELM frequency ν_{ELM} responds to density increase. For example, ν_{ELM} in the 14.3 MW cases *decreased* with density, while the ν_{ELM} for 10.3 MW cases *increased* (Fig. 3(b)).

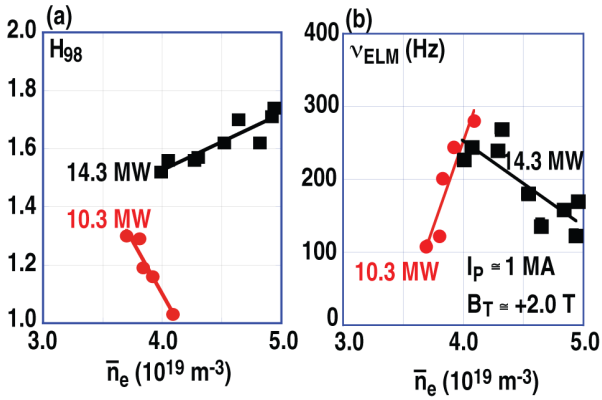

FIG. 3. (a) Normalized H-mode confinement time is shown as a function of line-averaged density at moderate and high power input P_{IN}. (b) The dependence of ELM frequency on line-averaged density is shown for moderate- and high P_{IN}.

These results have both positive and negative consequences for successful high power DND operation. D_2 gas injection at very high P_{IN} can raise H98 (and β_N) above "standard" expectation, which would be favorable for future high performance (DND) tokamaks. However, to reach the D^+ flow rates in the SOL needed for successful puff-and-pump operation would require D_2 gas puff rates that could well push core density above its target value, particularly since continued D_2 injection would be decreasing ν_{ELM} and improving H98 still further.

Figure 4 details how high performance DND plasmas respond to D_2 gas puffing at different P_{IN}. For the lower P_{IN} (≈11 MW) case shown in column 1, a low gas puff discharge (black) is overlaid on a higher gas puff case (red), shown in Fig. 4(a1). Line-averaged density increased 10-15% between t = 2.5 s – 4.5 s for moderate power input (P_{IN}, Fig. 4(b1,c1)). H98 dropped ≈10% (Fig. 4(d1)). Pedestal electron pressure ($P_{e,PED}$) decreased slightly (Fig. 4(e1)), while the ELM frequency near the end of the flattop was found to increase in the higher gas puffing

case, i.e., 180 Hz vs. 130 Hz. This behavior is typical of D_2 gas puffing cases for high performance DIII-D DND plasmas at lower and moderate P_{IN}.

Column 2 shows the evolution for plasmas with deuterium gas puffing rates similar to those in column 1 but at higher P_{IN} (≈14 MW). Between 2.5 s and 3.8 s, plasma density increased by ≈40% (Fig. 4(a2,b2,c2). H98 *increased* ≈10-15% (Fig. 4(d2)) and pedestal electron pressure increased by ≈50% (Fig 4(e2). ELM frequency *decreased* with increasing density from ≈210 Hz to ≈110 Hz (not shown).

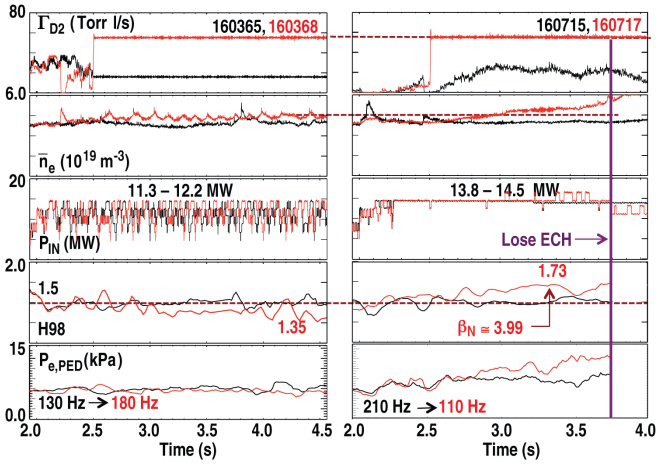

FIG. 4. Low (black) and high (red) D_2 gas puffing cases at lower power input and β_N (column 1) are compared with corresponding low (black) and high (red) D_2 gas puffing cases at high power input and β_N (column 2). (a) deuterium gas puff rates, (b) line-averaged density, (c) power input, (d) normalized energy confinement H98, and (e) pedestal electron pressure. Included in box (a5) and (b5) are the differences in ELM frequency at the end of the time intervals of interest for the lower (black) and the higher (red) gas puff rates. The drop in H98 at ≈3.5 s in box (d2) resulted from a brief period of counter-beam operation.

Analysis of the data indicates that, unlike high performance plasmas at lower P_{IN} where the H-mode pedestal density and temperature widths decreased with gas puffing [11], the widths of the density pedestal and the temperature pedestal profiles of the very highly powered DN high performance plasmas in this study were largely unchanged during D_2 puffing. This, in turn, should raise the pedestal pressure and would allow the edge pedestal gradient at the peeling limit to increase substantially. Bootstrap current would be suppressed due to increased collisionality.

This view is consistent with pedestal stability analysis using the ELITE code [12]. ELITE analysis demonstrates how differently the plasma pedestal respond to D_2 puffing at the two different power levels, i.e., 11 MW and 14 MW case in Fig. 5. For the lower powered, gas puffed case, ELITE indicated that the ballooning branch of the peeling-ballooning mode (PBM) would limit the pedestal pressure gradient with any attempted density increase (Fig. 5(a)). Here, J_N is the normalized edge current density and α is the normalized pedestal pressure gradient (~ β_N). However, in the higher power discharge (Fig. 5(b)), it is only the peeling branch of the PBM that is present and this allows a higher edge pedestal pressure gradient (and β_N) as density is raised. Thus, unlike the lower power case, ELITE shows that these high powered discharges have a very high ballooning limit and a peeling/kink current limit that increases as the pressure gradient increases. Our analysis at this point indicates that this increase in the critical pressure gradient with D_2 puffing was responsible for observed improvement in energy confinement. As shown in column (b) of Fig. 4, a density increase of 20% by gas puffing in one high power case raised both H98 and β_N by 10-15% to 1.7 and 4.0,

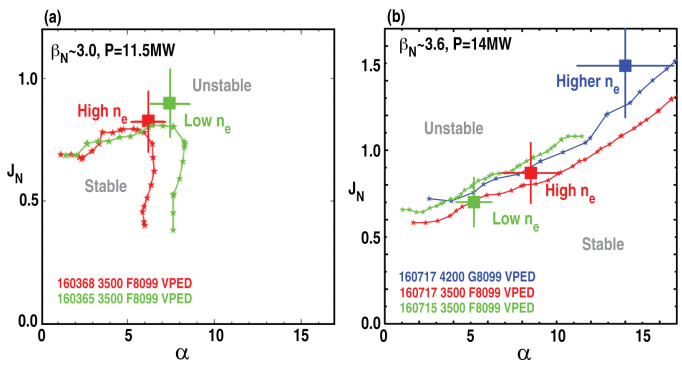

FIG. 5. ELITE stability diagram is shown for the moderate P_{IN} case (a) and the high P_{IN} case (b).

respectively.

At this time, we think that improved fueling of the main plasma clearly has a role in determining the density and temperature widths in the pedestal, which would allow access to higher stability regimes in the higher power case. In turn, this affects the ELMing, as in Fig. 3(b). A decreasing ν_{ELM} with increasing density in the 14 MW case would further improve plasma fueling and lower ELM frequency. Upcoming experiments on DIII-D will attempt to clarify the role of particle fueling in this phenomenon.

3.4 "Semi-slot" divertor

DIII-D at present does not have a divertor structure that fully encloses the outer divertor leg. However, recent data has provided an indication of how a high performance DND plasma might respond to a more tightly enclosed divertor leg. First, the outer divertor strike point is positioned adjacent to the 11-cm high baffle structure (circled, in Fig. 6(a)). This arrangement is referred to as a "semi-slot", because much of the outer divertor leg is "closed" on the low-field side but still completely "open" on the side facing the private flux region. In this case, the divertor flux enclosed by the semi-slot is 8 mm, as referenced to the outer midplane, which is about twice that of the heat flux width (≈3-4 mm, referenced to the midplane).

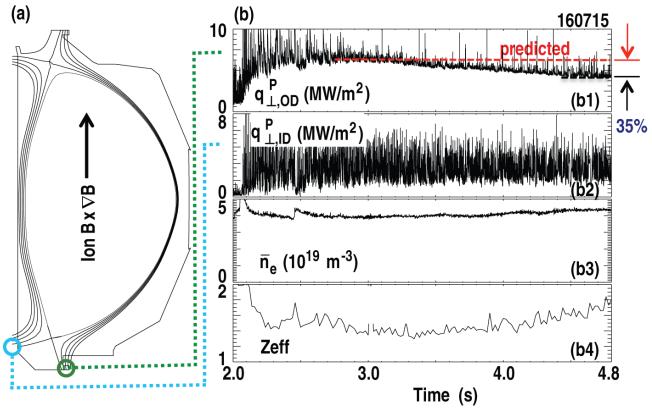

FIG. 6. (a) Cross-section of a high performance DND plasma with the location of the outer strike point adjacent to the baffle structure (green circle) and inner strike point on the centerpost (blue circle): P_{IN} = 14 MW, β_N = 3.7, H98 = 1.55, and $\Gamma_{D2} \leq 20$ torr l/s. (b1) The peak heat flux at the outer divertor target in the lower divertor ($q_{\perp,OD}^P$), (b2) Peak heat flux at the inner divertor target in the lower divertor ($q_{\perp,ID}^P$), (b3) line-averaged density, (b4) core plasma Zeff.

Figure 6(b1) shows $q_{\perp,OD}^P$ has reached its maximum at ≈2.5 s, corresponding to when the plasma shaping-related transients in this shot have largely subsided and the outer strike point is properly positioned. At this time $q_{\perp,OD}^P$ determined from the IRTV data was ≈5 MW/m^2; this is consistent with the predicted $q_{\perp,OD}^P$ based on the scaling from Fig. 2 (dashed red line in Fig. 6(b1). After 3 seconds, however, $q_{\perp,OD}^P$ decreased steadily and by t = 4.8 s, $q_{\perp,OD}^P \approx 3.2$ MW/m^2, a decrease of ≈35% from its initial value. At the same time, no decrease in the peak heat flux at the more open *inner* divertor target was observed, i.e., $q_{\perp,ID}$ ≈1.8 MW/m^2 (Fig. 6(b2). Plasma density increased ≈10% after 4.0 s (Fig. 6(b3)) when Zeff also showed an increase (Fig. 6(b4)).

The rise in both density and Zeff was largely due to carbon buildup. Figure 7 shows the averaged carbon density between ρ of 0.4 and 0.8 as a function of time for three distinct P_{IN}. The black squares in Fig. 7 represent shot 160715 described in Fig. 6(b). Similar high performance shots at higher and lower P_{IN} have been added for comparison. All three cases are identically prepared up to t = 2.8 s. Between 3.8 s and 4.0 s, the carbon content of the core plasma for the P_{IN} = 14 MW case began to increase, consistent with the activity observed for density and Zeff in Fig. 6(b3,b4). At least 75% of the rise in density between 3.8 s and 4.8 s was tied to the increase in the carbon content. However, the 10.8 MW case showed no evidence of an increase in carbon content in the core and in fact was decreasing near the end of flattop. Not surprisingly, the 16.4 MW case showed a stronger rise in carbon content than

the 14 MW case, although subsequent analysis showed that part of this increase was due to prompt local (counter-)beam ions losses sputtering carbon on the outer midplane wall.

The poloidal distribution of the CIII radiated power is useful in understanding the temporal behaviors of $q_{\perp,OD}^{P}$ and $q_{\perp,ID}^{P}$, as well as the likely source of the carbon buildup in the core in the 10.8- and 14 MW cases. Figure 8(a,b) shows the poloidal distributions of CIII radiated power in the 10.8 MW case (a) at an early time and (b) near the end of flattop. Likewise, Fig. 8(c,d) shows the same for the 14 MW case. These distributions are based on an inversion of data from a camera viewing the lower divertor tangentially through a CIII filter.

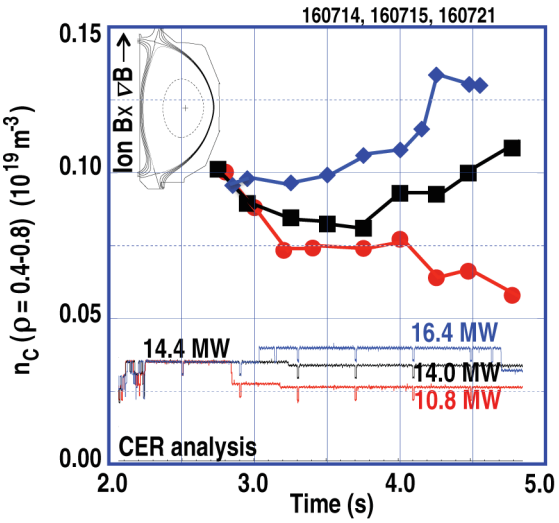

FIG. 7. High performance plasmas at P_{IN} = 10.8 MW, 14.0 MW, and 16.4 MW show carbon accumulation in the main plasma depends strongly on P_{IN}. Power input traces are overlaid. The three cases are identically prepared up to t = 2.8 s.

In the 10.8 MW case, changes in the CIII intensity peak between 3.0 s and 4.8 s were minor on the baffle top, i.e., at the entrance to the "semi-slot", and the bolometrically-determined radiated power from this same location showed virtually no increase. Yet, Fig. 8(a,b) shows that the CIII intensity peak at the lower outer divertor target increased significantly during this time. The 14 MW case also generated a similar increase in the CIII intensity peak at its outer target, but, unlike the 10.8 MW case, it also generated a significant increase in CIII activity at the semi-slot entrance as well; in this case, bolometrically-determined radiated power from the region around the semi-slot entrance showed a factor of ≈1.8 increase in radiated power. Note that the CIII radiated power at the lower inner divertor target was relatively low in both cases, and what increase there was between 3.0 s and 4.8 s was small.

These results suggest that (1) the buildup of carbon radiation at the outer strike point during the the 14 MW shot corresponded to the decrease in the peak heat flux shown in Fig. 6(b1), (2) the source of the carbon that was "fueling" the plasma originated on the baffle top above the outer strike point, i.e., the "entrance" to the semi-slot, and (3) since the CIII radiation was virtually unchanged at the *inner* divertor target between 3.0 s and 4.8 s, the peak heat flux at the inner divertor target was also unchanged, as in Fig. 6(b2). Though not shown, the peak heat flux at its outer divertor target in the 10.8 MW case also decreased in a manner similar to what was observed in the 14 MW case, consistent with the rise in CIII radiation at its outer divertor target.

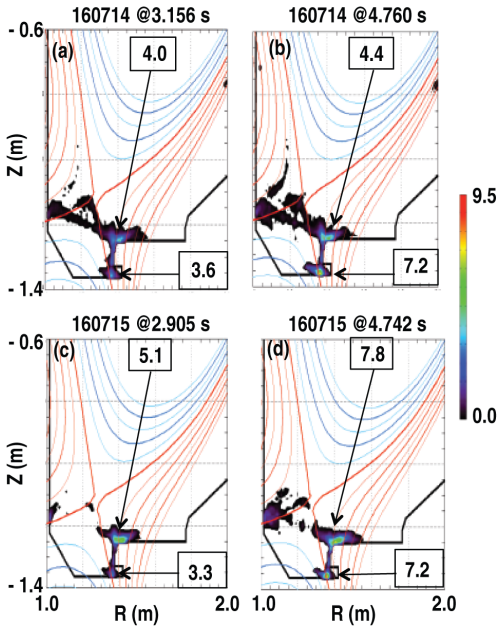

FIG. 8. The spatial distribution of the CIII radiation for two of the P_{IN}-cases shown in Fig. 7. P_{IN} = 10.8 MW: (a) early flattop and (b) late flattop. P_{IN} = 14.0 MW: (c) early flattop and (d) late flattop. The intensity peaks of each case at their respective outer strike points and on the baffle lip above the outer strike point (entrance to the "semi-slot") are indicated; the color bar is uncalibrated.

The above implies that the carbon neutrals/ions generated at the entrance to the semi-slot was an important source for carbon buildup in the plasma core in the 14 MW case. This interpretation has gained additional support more recently, when graphite tiles on the floor adjacent to the pump entrance were replaced by *tungsten-coated* tiles and significant carbon accumulation was still observed. Carbon neutrals/ions generated inside the semi-slot near the target were not a major source for the observed carbon accumulation but still had an important role in reducing the peak heat flux at the target.

4. Conclusions

The dependence of $q_{\perp,OD}^{P}$ on P_{SOL} and I_P was largely consistent with what would be expected from single-null plasmas from ITPA studies, even though the former were composed of high performance near-DND shaped plasmas and the latter with single-null H-mode plasmas.

Gas puffing into high-power high performance-plasmas yielded improved confinement. This result is favorable for future generation tokamaks that will rely on high energy confinement and plasma beta to be successful. The rise in density that accompanies this improved energy confinement may also be viewed favorably and, in fact, might even be considered as a useful tool in fueling. For contemporary tokamaks that rely on second harmonic EC heating, however, a significant improvement in fueling might not be viewed as favorably, because rising density can bend or reflect the RF beams and thereby restrict successful application of ECH to relatively low densities. In DIII-D, for example, possible damage to in-vessel components by reflected EC heating limits ECH use to lower densities, putting severe limitations on effective puff-and-pump operation. A more "closed" divertor that improves deuterium and impurity neutrals retention at or near the divertor target may be helpful in controlling plasma density by relaxing the gas injection requirements needed to reduce heat flux at the (enclosed) divertor target.

The "semi-slot" experiment was interesting from two aspects: (1) it showed that significant heat flux reduction was possible in the presence of graphite divertor armor, even in a semi-slot without significant D_2 puffing and (2) it strongly suggested that care must be taken in properly contouring the opening to the slot. Carbon sputtered off the graphite tiles near the outer target played an important role in reducing the peak heat flux. Future high-powered tokamaks, however, will not be using graphite armor, so that selecting the appropriate seed impurity will be important. While impurities like nitrogen or argon were shown to be appropriate for highly powered DIII-D conditions, higher-Z impurities would certainly be used for a DEMO.

Work supported by the U.S. Department of Energy under DE-FC02-04ER54698[1], DE-AC52-07NA27344[2], DE-FG02-04ER54761[3], and DE-AC04-94AL85000[4]. DIII-D data shown in this paper can be accessed at https://fusion.gat.com/global/D3D_DMP.

References

[1] WADE, M.R., et al., Nucl. Fusion **38** (1998) 1839.
[2] GOETZ, J.A., et al., J. Nucl. Mater. **266-269** (1999) 359.
[3] KALLENBACH, A., et al., J. Nucl. Mater. **337–339** (2005) 732.
[4] PETRIE, T.W., et al., J. Nucl. Mater. **363-365** (2007) 416.
[5] PETRIE, T.W., et al., J. Nucl. Mater. **463** (2015) 1225.
[6] PETRIE, T.W., et al., Nucl. Fusion **53** (2013) 113024.
[7] RYUTOV, D.D., Phys. Plasmas **14** (2007), 064502.
[8] SOUKHANOVSKII, V.A., et al., Phys. Plasmas **19** (2012) 082504.
[9] KOTSCHENREUTHER, M., Phys. Plasmas **14** (2007) 072502.
[10] EICH, T., et al., IAEA-FEC (2012) San Diego.
[11] LEONARD, A.W., et al., J. Nucl. Mater. **463** (2015) 519.
[12] SNYDER, P.B., et al., Phys. Plasmas 9 (2002) 2037.